Supporting Information

In situ dual growth of graphitic structures in biomass carbon to yield a potassium-ion battery anode with high initial coulombic efficiency

Zheren Tang [a,b,*], Yan Wang [c], Zheng Zheng [a,b,*] and Xingzhang Luo [a,b,*]

a. Department of Environmental Science and Engineering, Fudan University, Shanghai 200438, People's Republic of China

b. Research Centre for Watershed Pollution Control, Fudan University, Shanghai 200438, People's Republic of China

c. Department of Materials Science, Fudan University, Shanghai 200433, People's Republic of China

E-mail: zzhenghj@fudan.edu.cn (Z. Zheng)

E-mail: lxz@fudan.edu.cn (X. Luo)

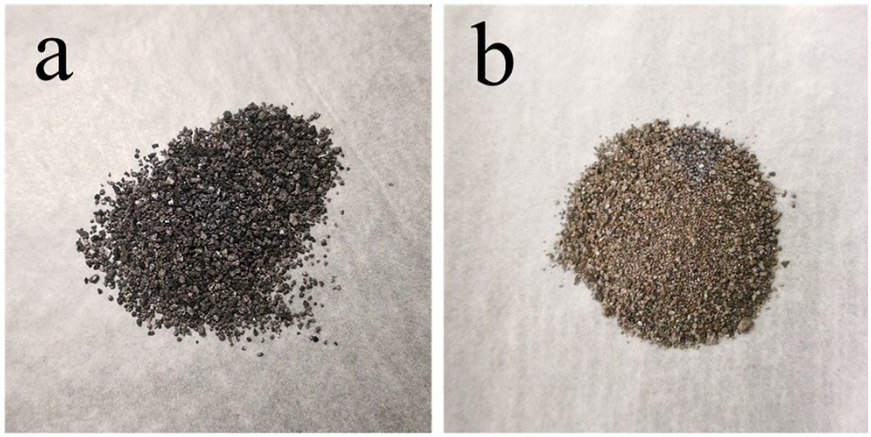

Figure S1. Photos of (a) petroleum coke pellet and (b) template pellet.

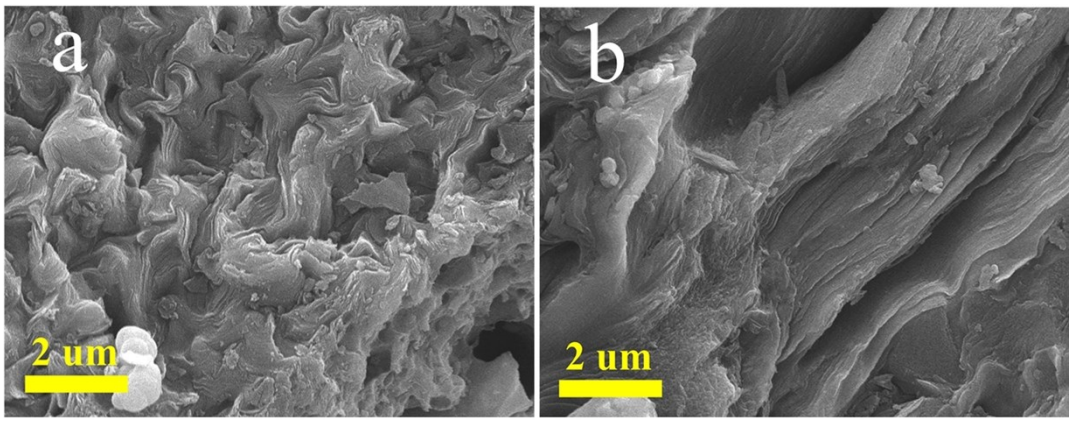

Figure S2. SEM images of template pellet: (a) before and (b) after carbonization.

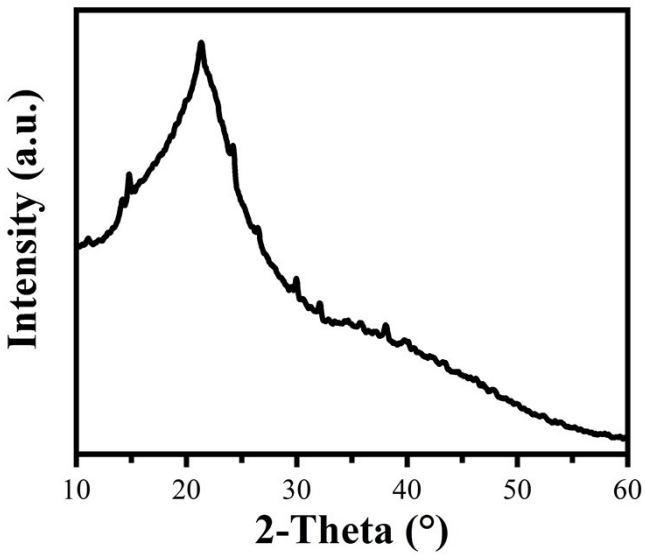

Figure S3. XRD pattern of tea-waste powder separating from the mixture of tea-waste and template pellet.

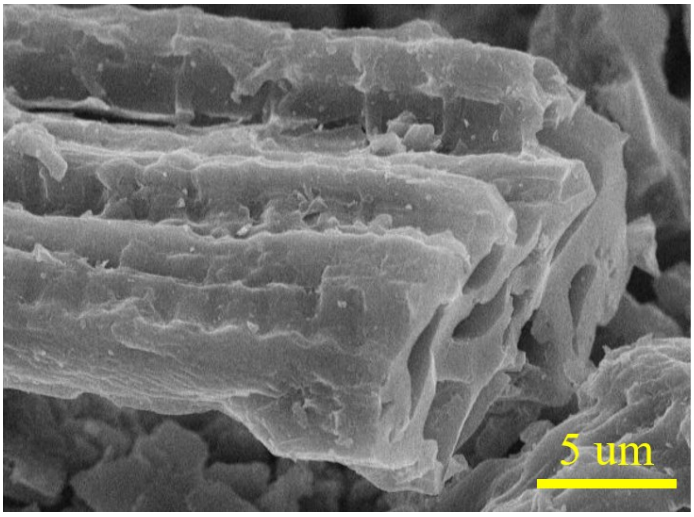

Figure S4. SEM image of TWC-SC-G sample showing the morphology.

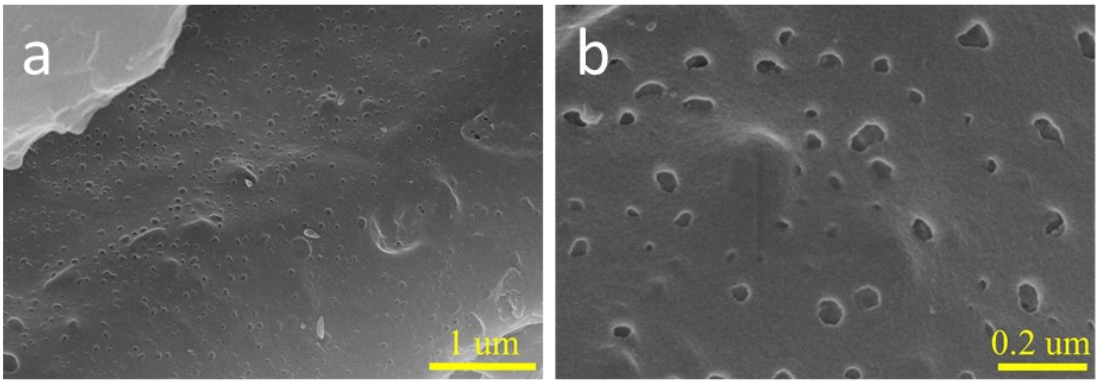

Figure S5. SEM images of TWC-SC-G sample showing the pore structure: (a) low magnification and (b) high magnification.

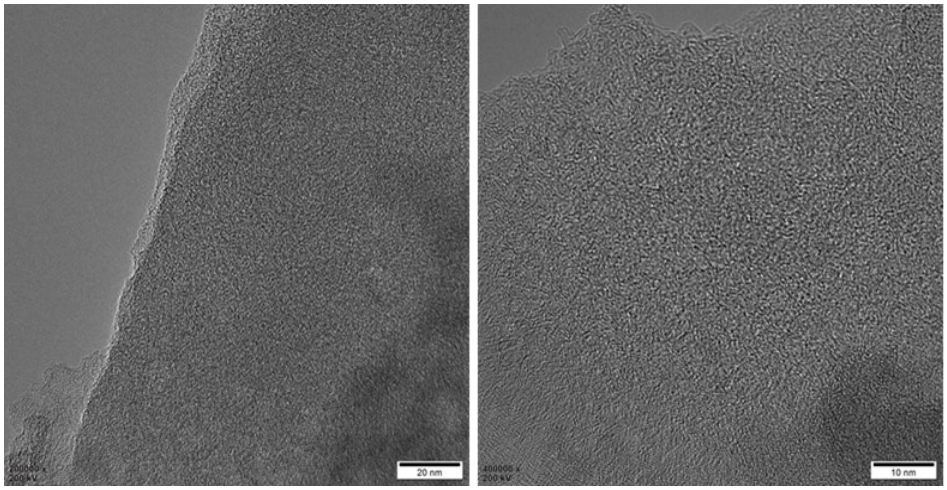

Figure S6. TEM images of TWC-SC sample.

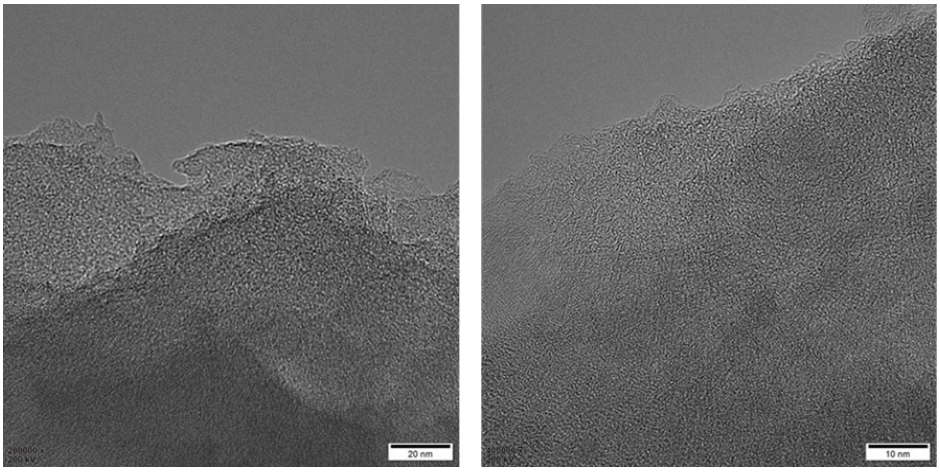

Figure S7. TEM images of TWC-H sample.

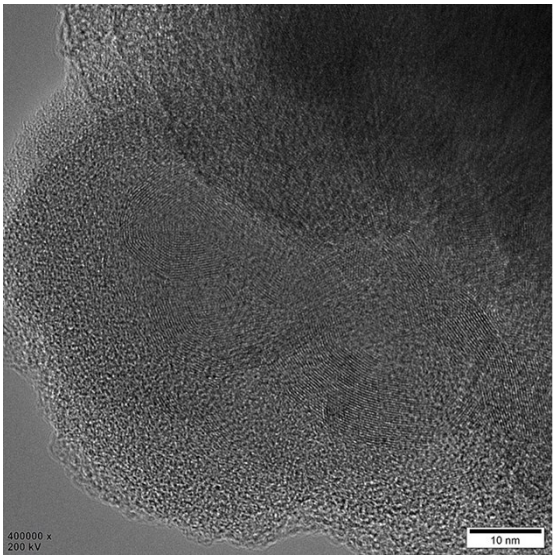

Figure S8. TEM image of TWC-G sample.

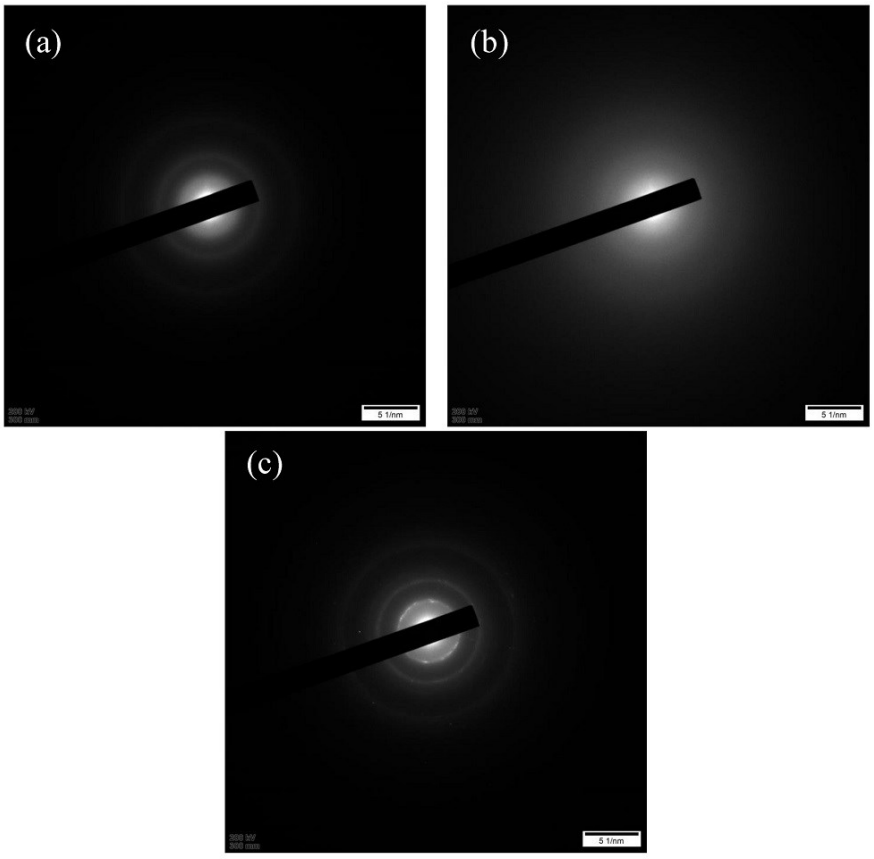

Figure S9. SAED patterns of (a) TWC-SC, (b) TWC-H and (c) TWC-G samples.

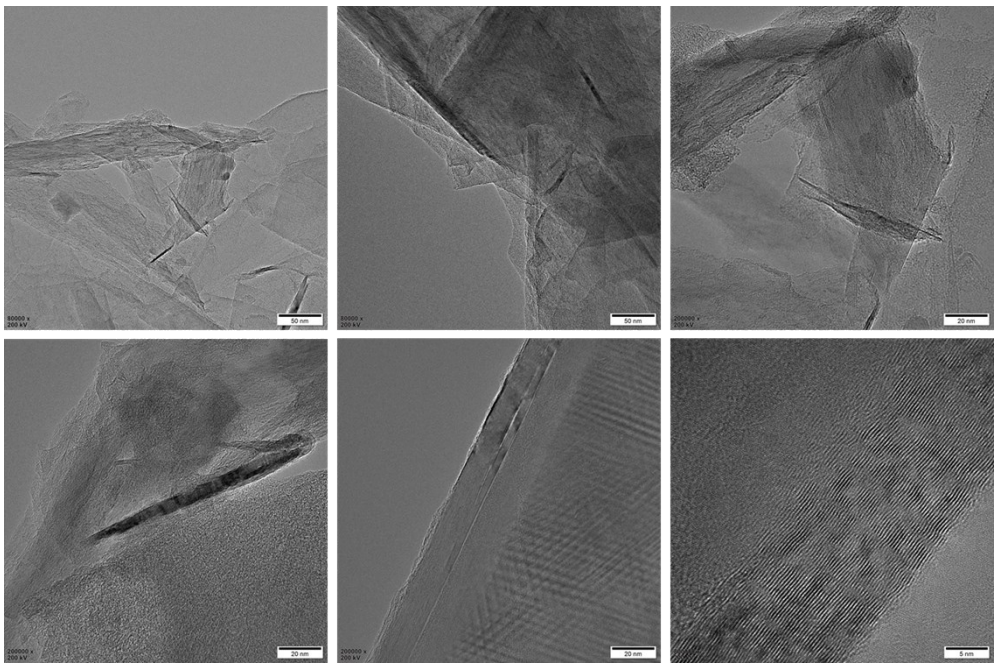

Figure S10. TEM and HRTEM images of the graphitic structures in TWC-SC-G sample showing the repeatability.

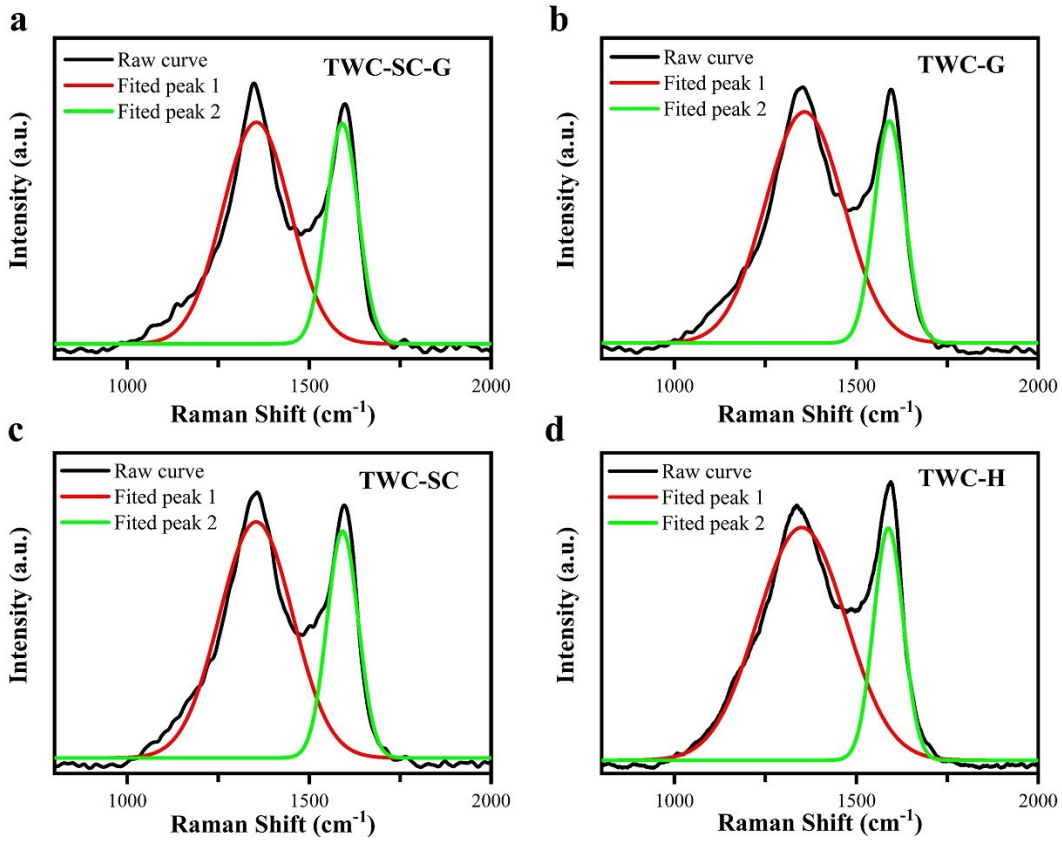

Figure S11. The fitted results in Raman patterns of (a) TWC-SC-G, (b) TWC-G, (c) TWC-SC, and (d) TWC-H samples.

Table S1. BET specific surface area, pore size and pore volume of 4 TWC samples

Sample	BET specific surface area ($m^2 \cdot g^{-1}$)	Average pore size (nm)	Total pore volume ($cm^3 \cdot g^{-1}$)	Micro pore volume ($cm^3 \cdot g^{-1}$)
TWC-SC-G	182.4	2.11	0.09	0.06
TWC-SC	50.5	2.93	0.02	<0.01
TWC-H	24.9	2.56	0.03	0.01
TWC-G	191.0	1.91	0.11	0.08

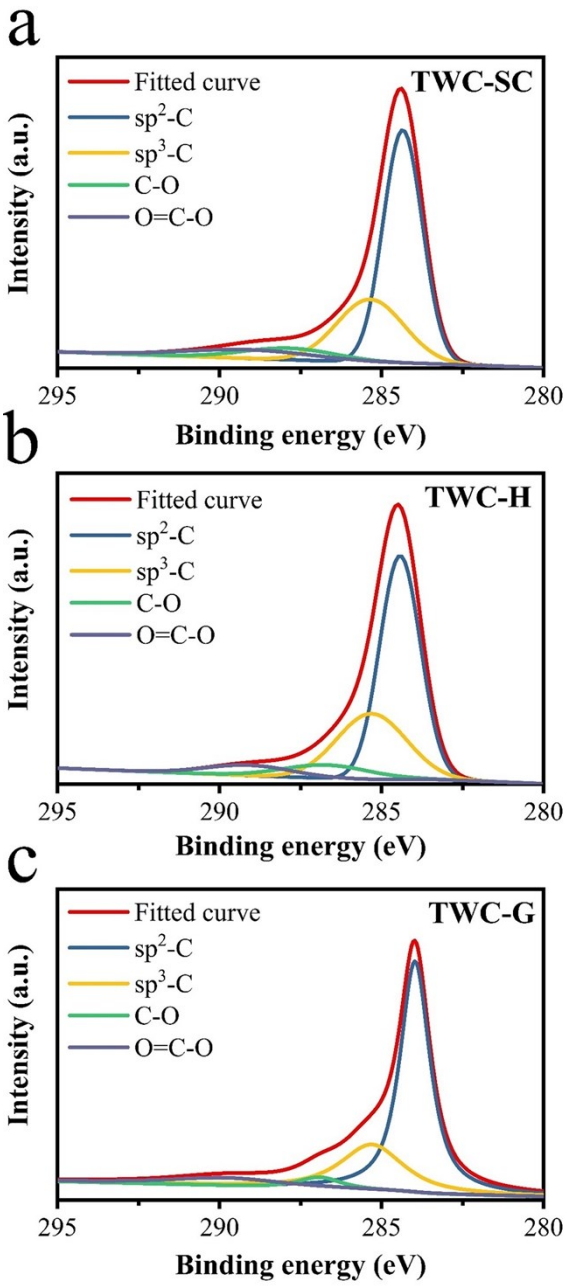

Figure S12. C1s XPS spectrum of (a) TWC-SC, (b) TWC-H and (c) TWC-G samples.

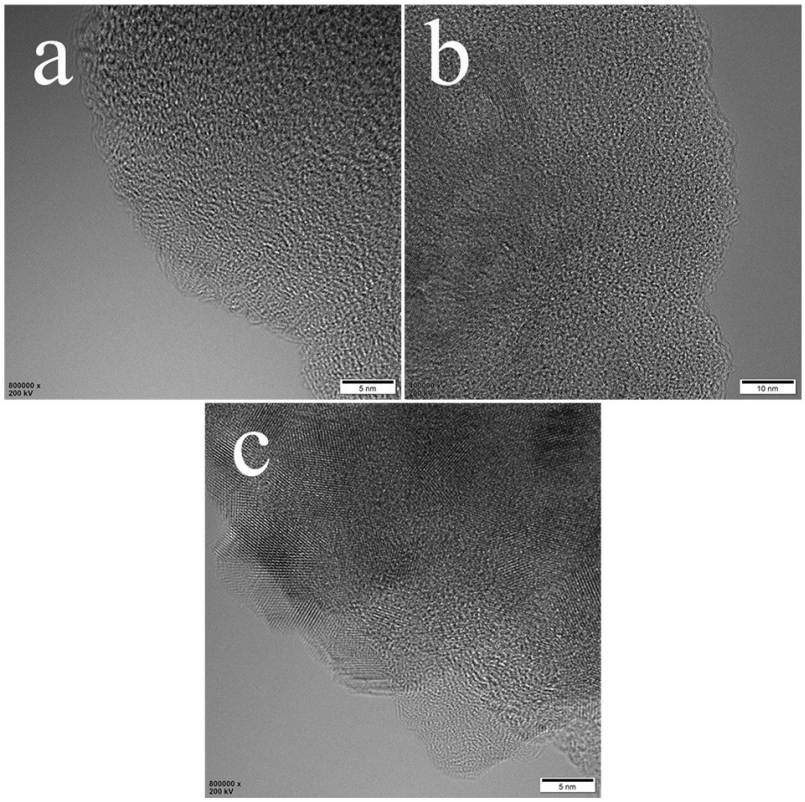

Figure S13. TEM images of carbonized tea-waste powder annealing with template pellet together at given temperatures: (a) 600 ^{o}C, (b) 800 ^{o}C and (c) 1000 ^{o}C.

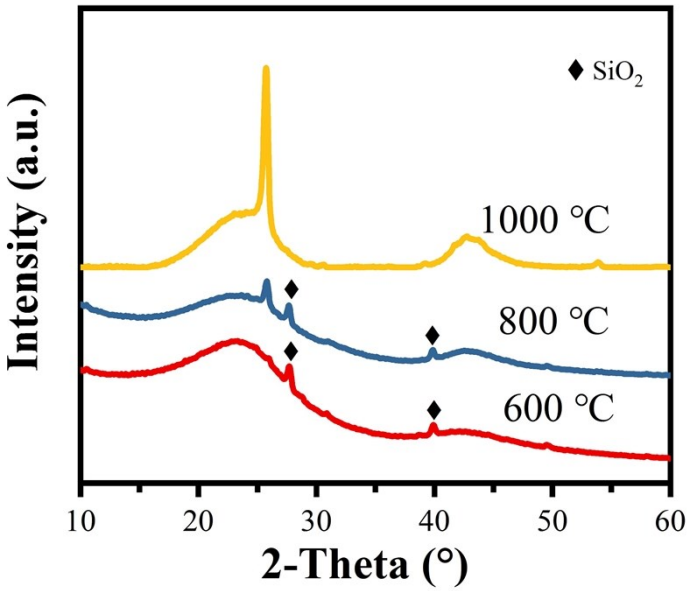

Figure S14. XRD patterns of carbonized tea-waste powder annealing with template pellet together at given temperatures: (a) 600 °C, (b) 800 °C and (c) 1000 °C.

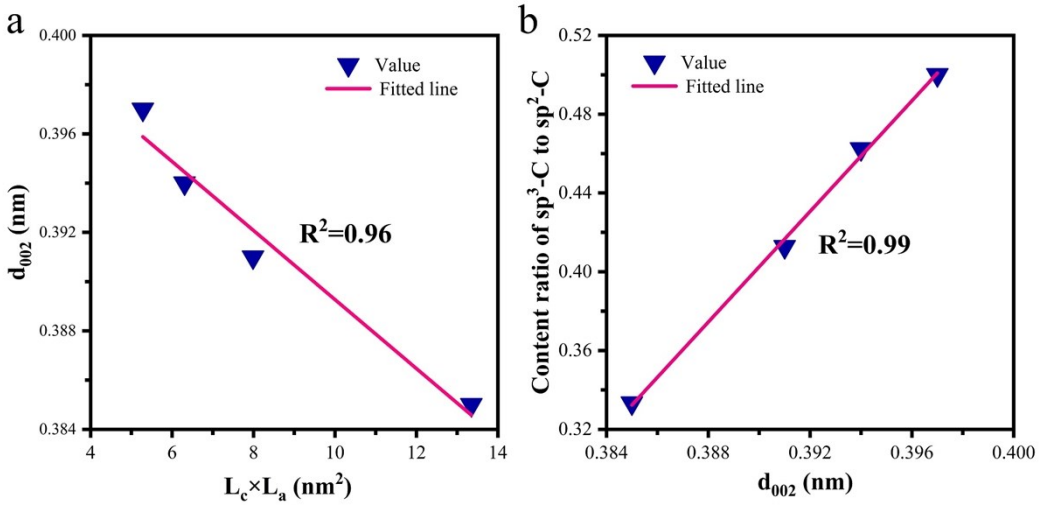

Figure S15. The linear relationship between (a) $L_c \times L_a$ and d_{002}, and (b) d_{002} and the content ratio of sp^3-C to sp^2-C.

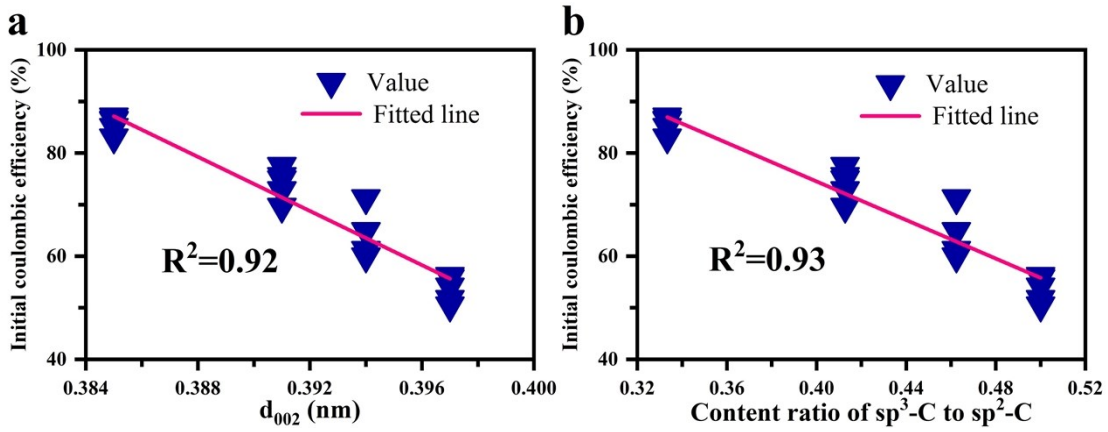

Figure S16. The linear relationship between ICE and (a) d_{002} and (b) the content ratio of sp^3-C to sp^2-C.

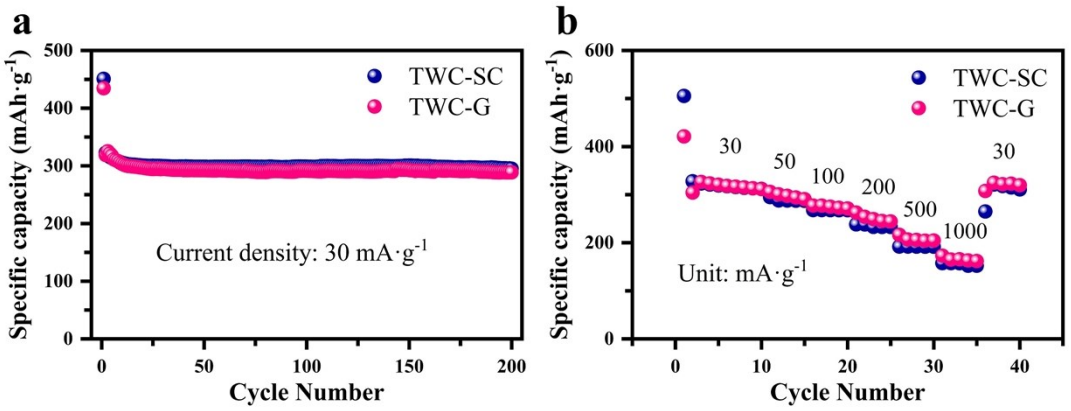

Figure S17. (a) Cycle and (b) Rate performance of TWC-SC and TWC-G electrodes as KIB anodes.

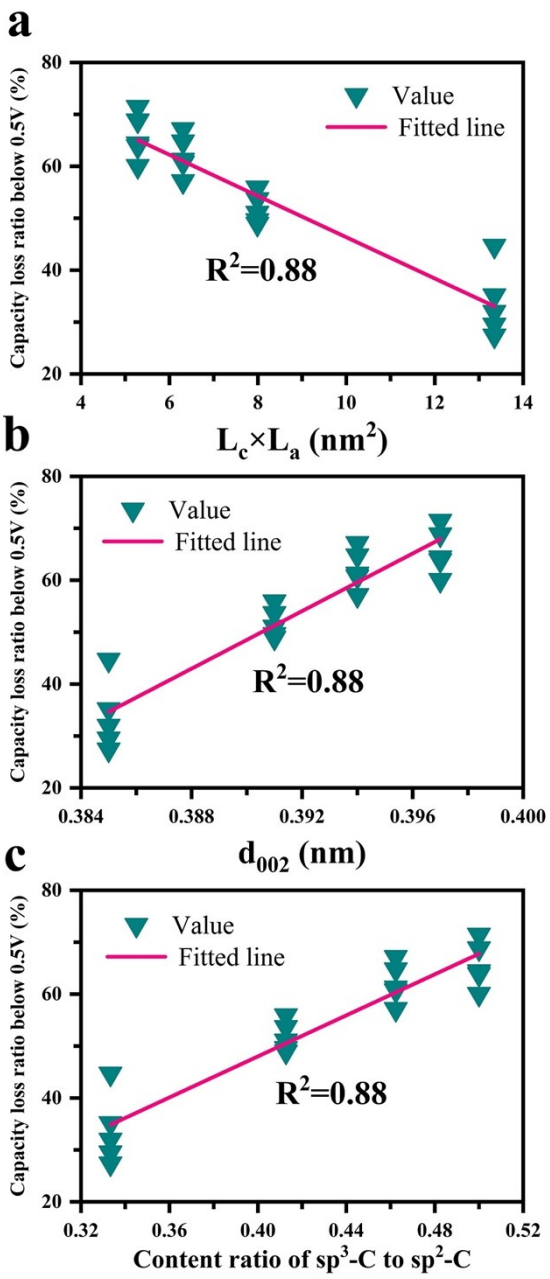

Figure S18. The linear relationship between capacity loss ratio below 0.5V with (a) $L_c \times L_a$, (b) d_{002}, and (c) the content ratio of sp^3-C to sp^2-C.

Capacity loss ratio below 0.5V=

1-1st charge capacity under 0.5V/1st discharge capacity under 0.5V

Table S2. The elemental content of the 4 TWC samples based on XPS data

Sample	Elemental content (%)		
	C1s	**O1s**	**N1s**
TWC-SC-G	93.8	5.6	0.6
TWC-G	92.8	6.5	0.7
TWC-SC	90.9	8.0	1.1
TWC-H	88.9	10.5	0.6

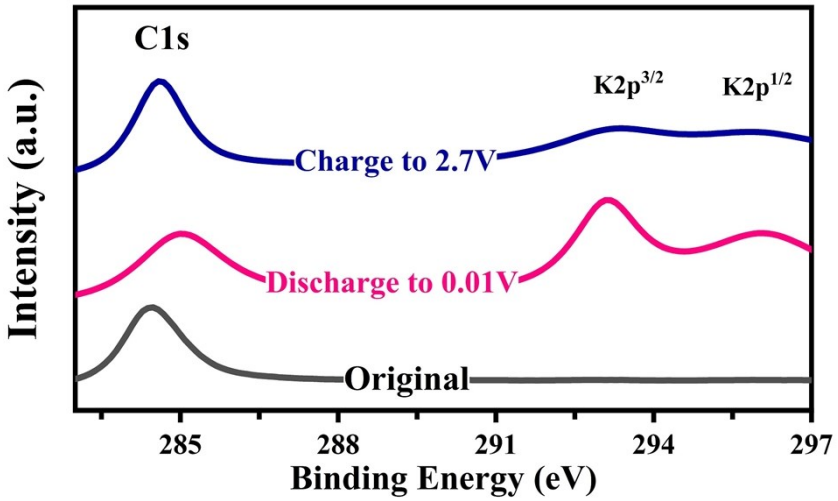

Figure S19. XPS spectra of TWC-SC-G electrode at different discharge/charge stages during the first cycle.

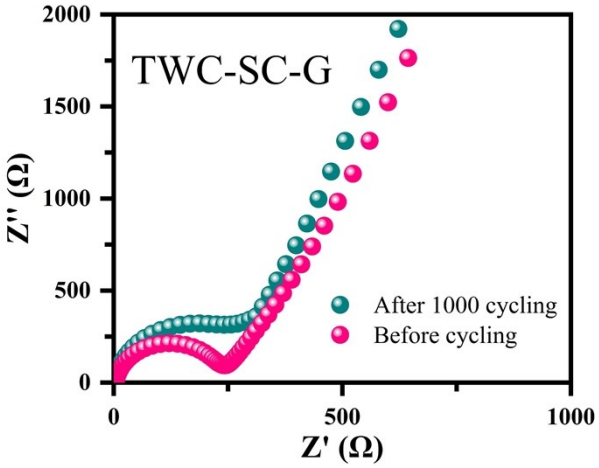

Figure S20. EIS curves of TWC-SC-G electrodes before cycling and after 1000 cycling.

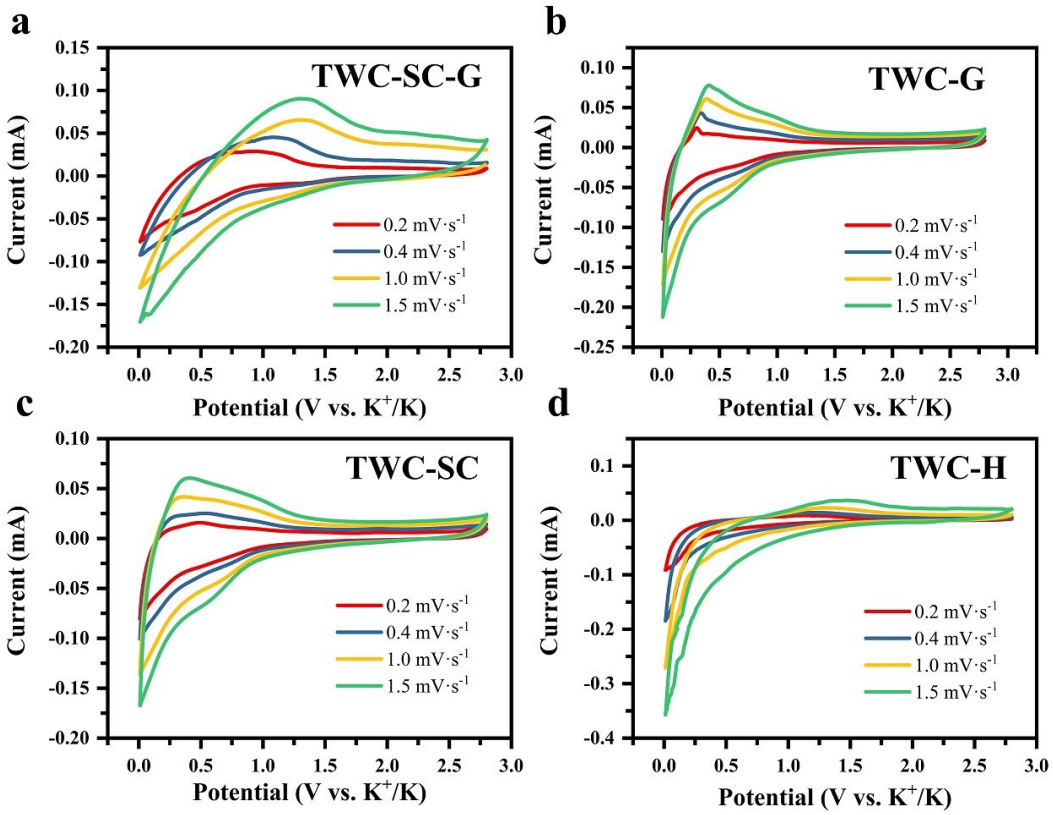

Figure S21. CV curves of (a) TWC-SC-G, (b) TWC-G, (c) TWC-SC and (d) TWC-H electrodes as KIB anodes at different scan rates.

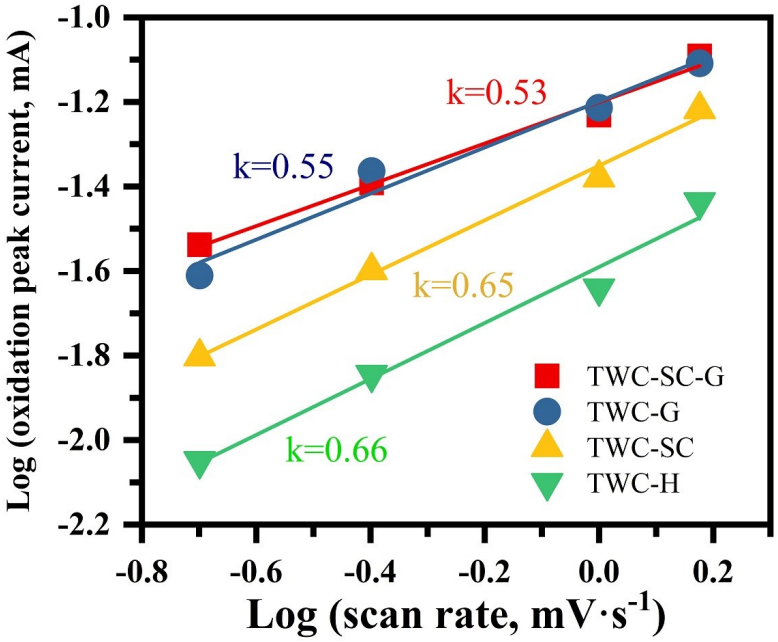

Figure S22. The liner relationship between the logarithm of oxidation peak current and the logarithm of scan rate in charge process for the 4 TWC electrodes as KIB anodes.

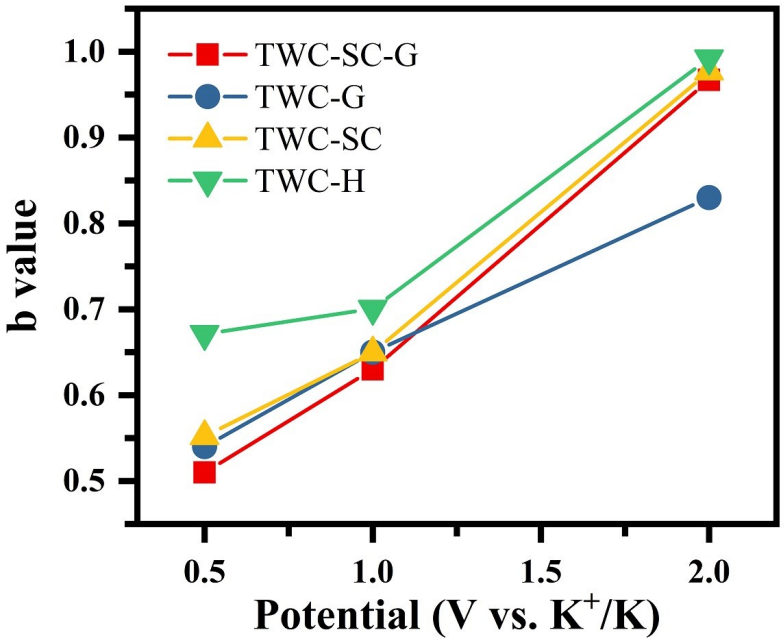

Figure S23. The b values at given potentials in discharge process for the 4 TWC electrodes as KIB anodes.

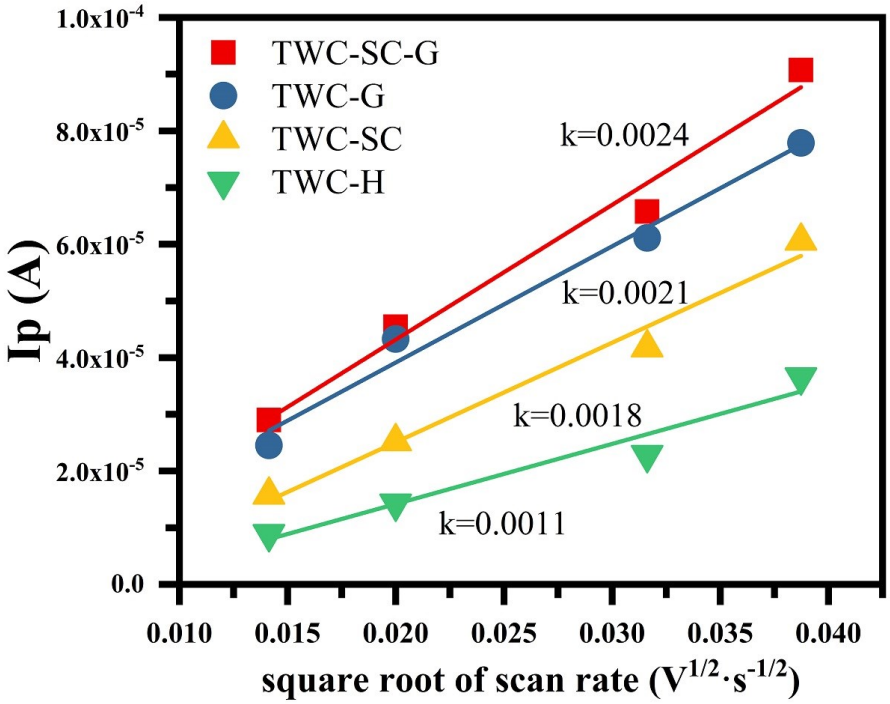

Figure S24. The liner relationship between the oxidation peak current and the square root of scan rate for the 4 TWC electrodes as KIB anodes.

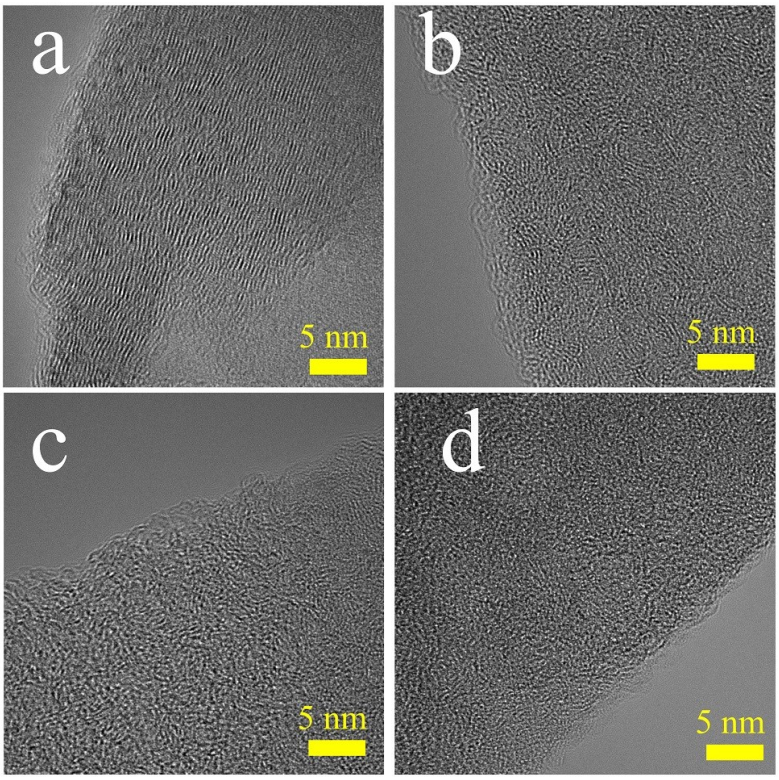

Figure S25. HRTEM images of (a) TWC-SC-G, (b) TWC-G, (c) TWC-SC and (d) TWC-H electrodes after 1000 cycles.

Table S3. Electrochemical performance of carbon-based materials as anode in KIBs

Material	Electrolyte	Current Density ($mA \cdot g^{-1}$)	Capacity ($mAh \cdot g^{-1}$)	ICE	Capacity retention/cycle numbers	Reference
Biomass hard carbon with graphitic structures	1 M KPF_6 in DME	30	367	85.6%	98%/200	**This work**
		100	322		93%/200	
		1000	235		94%/1000	
Nitrogen-doped carbon microsphere	0.8 M KPF_6 in EC: DEC=1:1 by volume	~33.6	~250	~76%	~82%/200	1
		~504	~180		~94%/4000	
Hard-Soft composite carbon	0.8 M KPF_6 in EC: DEC=1:1 by volume	27.9	261	67%	93%/200	2
Expanded graphite	1 M KFSI in EC: DEC=1:1 by volume	50	202	81.6%	105.1%/200	3
		200	175		99.4%/500	
Commercial graphite	1 M KFSI in EC: DEC=1:1 by volume	50	169	80.8%	36.1%/200	3
		200	44		-	
S/O co-doped porous carbon microspheres	0.8 M KPF_6 in EC: DEC=1:1 by volume	50	230	~60%	98.5%/100	4
		1000	158		81.5%/2000	
Potato derived biomass porous carbon	3 M KFSI in DME	100	270	42.6%	91.8%/100	5
		500	200		87.5%/200	
N-doped hierarchical porous carbon	0.8 M KPF_6 in EC: DEC=1:1 by volume	100	264	55.1	92%/200	6
Graphitic carbon nanocage	1 M KFSI in EC: PC=1:1 by volume	55.8	212	40%	92%/100	7
Petroleum coke-Artemisia Hedinii	0.8 M KPF_6 in EC: DEC=1:1 by volume	~69.8	116	25.5%	94.5%/500	8
Oak hard carbon synthesized at 1100°C	0.4 M KPF_6 in EC: DEC=1:1 by volume	100	135	56%	94%/150	9
Pyridinic N-content-doped porous carbon monolith	0.8 M KPF_6 in EC: DEC=1:1 by volume	100	319	~20%	77%/120	10
		1000	225		~76%/3000	
Highly disordered hard carbon derived from skimmed cotton	1 M KPF_6 in DME	200	240	73%	92%/150	11
		4000	165		-	
Carbon nanofiber foam derived from bacterial cellulose	1 M KPF_6 in EC: DMC: EMC=4:3:2 by volume	200	202	<30%	83%/100	12

Ordered mesoporous carbon	0.8 M KPF_6 in EC: DEC=1:1 by volume	50	286.4	63.6%	~90%/100	13
		1000	144.2		~70%/1000	
Nitrogen/Oxygen dual-doped hierarchical porous hard carbon	1 M KPF_6 in EC: DMC=1:1 by volume	50	315	25%	76.1%/100	14
		1050	174		~71.7%/1100	
Nitrogen/Oxygen co-doped hierarchically porous carbon	0.8 M KPF_6 in EC: DMC=1:1 by volume	50	352	38.7%	76%/100	15
Loofah-derived carbon	1 M KPF_6 in EC: DMC=1:1 by volume	100	225	~38%	-	16
Nitrogen/Oxygen codoped carbon hollow multihole bowls	0.8 M KPF_6 in EC: DMC=1:1 by volume	100	377	~60%	~81%/150	17
		1000	216		~62%/1000	
Biowaste orange peel-derived mesoporous carbon	0.75 M KPF_6 in EC: DMC=1:1 by volume	30	236	55%	~88%/100	18
Cotton-derived oxygen/sulfur co-doped hard carbon	1 M KPF_6 in DME	100	409	46.4%	-	19
		2000	135		~86%/500	

References

1. C. Chen, Z. Wang, B. Zhang, L. Miao, J. Cai, L. Peng, Y. Huang, J. Jiang, Y. Huang, L. Zhang and J. Xie, *Energy Storage Materials*, 2017, **8**, 161-168.
2. Z. Jian, S. Hwang, Z. Li, A. S. Hernandez, X. Wang, Z. Xing, D. Su and X. Ji, *Advanced Functional Materials*, 2017, **27**, 1700324.
3. Y. An, H. Fei, G. Zeng, L. Ci, B. Xi, S. Xiong and J. Feng, *Journal of Power Sources*, 2018, **378**, 66-72.
4. M. Chen, W. Wang, X. Liang, S. Gong, J. Liu, Q. Wang, S. Guo and H. Yang, *Advanced Energy Materials*, 2018, **8**, 1800171.
5. W. Cao, E. Zhang, J. Wang, Z. Liu, J. Ge, X. Yu, H. Yang and B. Lu, *Electrochimica Acta*, 2019, **293**, 364-370.
6. C. Gao, Q. Wang, S. Luo, Z. Wang, Y. Zhang, Y. Liu, A. Hao and R. Guo, *Journal of Power Sources*, 2019, **415**, 165-171.
7. B. Cao, Q. Zhang, H. Liu, B. Xu, S. Zhang, T. Zhou, J. Mao, W. K. Pang, Z. Guo, A. Li, J. Zhou, X. Chen and H. Song, *Advanced Energy Materials*, 2018, **8**, 1801149.
8. J. Shan, J. Wang, P. Kiekens, Y. Zhao and J. Huang, *Solid State Sciences*, 2019, **92**, 96-105.
9. S. J. R. Prabakar, S. C. Han, C. Park, I. A. Bhairuba, M. J. Reece, K.-S. Sohn and M. Pyo, *Journal of the Electrochemical Society*, 2017, **164**, A2012-A2016.
10. Y. Xie, Y. Chen, L. Liu, P. Tao, M. Fan, N. Xu, X. Shen and C. Yan, *Advanced Materials*, 2017, **29**, 1702268.
11. X. He, J. Liao, Z. Tang, L. Xiao, X. Ding, Q. Hu, Z. Wen and C. Chen, *Journal of Power Sources*, 2018, **396**, 533-541.

12. H. Li, Z. Cheng, Q. Zhang, A. Natan, Y. Yang, D. Cao and H. Zhu, *Nano Letters*, 2018, **18**, 7407-7413.
13. W. Wang, J. Zhou, Z. Wang, L. Zhao, P. Li, Y. Yang, C. Yang, H. Huang and S. Guo, *Advanced Energy Materials*, 2018, **8**, 1701648.
14. J. Yang, Z. Ju, Y. Jiang, Z. Xing, B. Xi, J. Feng and S. Xiong, *Advanced Materials*, 2018, **30**, 1700104.
15. Y. Sun, H. Xiao, H. Li, Y. He, Y. Zhang, Y. Hu, Z. Ju, Q. Zhuang and Y. Cui, *Chemistry-a European Journal*, 2019, **25**, 7359-7365.
16. Z. Wu, L. Wang, J. Huang, J. Zou, S. Chen, H. Cheng, C. Jiang, P. Gao and X. Niu, *Electrochimica Acta*, 2019, **306**, 446-453.
17. Z. Zhang, B. Jia, L. Liu, Y. Zhao, H. Wu, M. Qin, K. Han, W. Wang, K. Xi, L. Zhang, G. Qi, X. Qu and R. V. Kumar, *ACS Nano*, 2019, **13**, 11363-11371.
18. R. Verma, Y. N. Singhbabu, P. N. Didwal, A. G. Nguyen, J. Kim and C. J. Park, *Batteries & Supercaps*, 2020, **3**, 1099-1111.
19. B. Xu, S. Qi, F. Li, X. Peng, J. Cai, J. Liang and J. Ma, *Chinese Chemical Letters*, 2020, **31**, 217-222.